Dynamics of Spheroid Self-Assembly in Liquid-Overlay Culture of DU 145 Human Prostate Cancer Cells

Richard M. Enmon Jr.,[1,2] Kim C. O'Connor,[1,2,4,5] Daniel J. Lacks,[1] Daniel K. Schwartz,[1,3] Robert S. Dotson[6]

[1]Department of Chemical Engineering, Tulane University, Lindy Boggs Center, Suite 300, New Orleans, Louisiana 70118; telephone: 504-865-5740; fax: 504-865-6744; e-mail: koc@tulane.edu
[2]Interdisciplinary Program in Molecular and Cellular Biology, Tulane University, New Orleans, Louisiana
[3]Department of Chemistry, Tulane University, New Orleans, Louisiana
[4]Tulane Cancer Center, Tulane University School of Medicine, New Orleans, Louisiana
[5]Department of Surgery, Tulane University School of Medicine, New Orleans, Louisiana
[6]Department of Neurophysiology, Tulane University School of Medicine, New Orleans, Louisiana

Received 15 May 2000; accepted 28 September 2000

Abstract: The in vitro self-assembly of multicellular spheroids generates highly organized structures in which the three-dimensional structure and differentiated function frequently mimic that of in vivo tissues. This has led to their use in such diverse applications as tissue regeneration and drug therapy. Using Smoluchowski-like rate equations, herein we present a model of the self-aggregation of DU 145 human prostate carcinoma cells in liquid-overlay culture to elucidate some of the physical parameters affecting homotypic aggregation in attachment-dependent cells. Experimental results indicate that self-aggregation in our system is divided into three distinct phases: a transient reorganization of initial cell clusters, an active aggregation characterized by constant rate coefficients, and a ripening phase of established spheroid growth. In contrast to the diffusion-controlled aggregation previously observed for attachment-independent cells, the model suggests that active aggregation in our system is reaction-controlled. The rate equations accurately predict the aggregation kinetics of spheroids containing up to 30 cells and are dominated by spheroid adhesive potential with lesser contributions from the radius of influence. The adhesion probability increases with spheroid size so that spheroid–spheroid adhesions are a minimum of 2.5 times more likely than those of cell–cell, possibly due to the upregulation of extracellular matrix proteins and cell-adhesion molecules. The radius of influence is at least 1.5 to 3 times greater than expected for spherical geometry as a result of ellipsoidal shape and possible chemotactic or Fröhlich interactions. Brownian-type behavior was noted for spheroids larger than 30 μm in diameter, but smaller aggregates were more motile by as much as a factor of 10 for single cells. The model may improve spheroid fidelity for existing applications of spheroids and form the basis of a simple assay for quantitatively evaluating cellular metastatic potential as well as therapies that seek to alter this potential. © 2001 John Wiley & Sons, Inc. *Biotechnol Bioeng* **72**: 579–591, 2001.
Keywords: spheroid; DU 145; prostate cancer; aggregation; kinetics; model

Correspondence to: Kim O'Connor
Contract grant sponsor: NASA; Tulane Cancer Center
Contract grant number: NAG 9-826

INTRODUCTION

Cell self-assembly into multicellular spheroids offers highly organized in vitro structures with in vivo-like fidelity. Spheroid cultures mimic both the three-dimensional organization and differentiated function of intact tissues to a much greater extent than do cell monolayers (Becker et al., 1993). This has led to their use in studies of basic biology, tissue regeneration, and drug/gene therapy. Spheroid culture is able to maintain a differentiated phenotype with enhanced liver-specific functions in cultured hepatocytes (Lazar et al., 1995), to induce differentiated function in stem cells and established lines (O'Connor et al., 1997; Sauer et al., 1997), and to establish the increased chemotoxic and radiographic resistance of several tumor lines to observed in vivo levels (Schwachöfer et al., 1991).

The most basic method of promoting spheroidal growth is liquid-overlay culture. Cell suspensions are grown in a static culture over an attachment-limiting surface such as agarose or agar (Yuhas et al., 1977). This promotes cell–cell attachment over attachment to the substratum. There has been extensive research describing the mechanisms by which the structural architecture of spheroids induces cell differentiation; increased cell–cell and cell-matrix interactions, changes in cell shape, and the development of a rich interstitial fluid within cell multilayers are essential in this regard (Durand, 1990; Sacks et al., 1989). In contrast, the

© 2001 John Wiley & Sons, Inc.

underlying mechanisms governing spheroidal formation remain poorly understood. Many seemingly promising cell lines are later found to be unable to self-assemble into spheroids (Sutherland, 1988).

Kinetic models of cellular aggregation based on Smoluchowski-like rate equations may be useful in elucidating mechanisms of spheroid self-assembly (Smoluchowski, 1917). In eukaryotic systems this approach has described the aggregation of both erythrocytes and Jurkat cells under static conditions (Neelamegham et al., 1997; Samsel and Perelson, 1982, 1984). To date however, the systems chosen allow simplifications to be made to the mathematical model based on the limited size or durability of the aggregates, the terminally differentiated state of the cells involved in aggregation, or the necessity of a catalyst for aggregation.

This study seeks to develop a mathematical model for cellular aggregation of DU 145 cells in liquid-overlay cultures. DU 145 cells are an established line of human prostate cancer cells that can self-assemble into large, stable spheroids through a combination of intracellular communication and diffusion. We propose a general model that is applicable to any self-aggregating system. Several complimentary versions of the model were developed that differ in the extent to which spheroid size was resolved. All models were able to accurately predict the aggregation kinetics of DU 145 cells during active self-assembly with a minimum number of variables. New insight was gained into the mechanisms governing spheroid formation by comparing model results with those generated using Smoluchowski's assumptions for ideal aggregation. In the future, the model may improve spheroid fidelity for existing applications and form the basis of a simple assay for quantitatively evaluating metastatic potential.

MATERIALS AND METHODS

Cell Cultivation

DU 145 cells (ATCC HTB 81, Rockville, MD) were propagated at 37°C, 95% relative humidity, and 5% CO_2 in GTSF-2 medium (Lelkes et al., 1997) at pH 7.4 containing 7% fetal bovine serum. Liquid-overlay plates were prepared from 60 × 15 mm petri dishes (Becton Dickinson Labware, Franklin Lakes, NJ) containing 3-mL serum-free GTSF-2 solidified with 1% agar (Difco, Detroit, MI). A 3-mL liquid overlay of complete GTSF-2 medium was seeded at 2×10^4 cell/cm^2 from trypsinized stock T-flask cultures of DU 145 cells. For extended culture, 3 mL fresh medium was added on the second day. This allowed for replacement of spent medium at the air–liquid interface without disturbing the cellular layer on the agar surface. Half of the cell-free overlay was replaced every other day to maintain the glucose concentration between 0.90 and 1.30 g/L, and pH between 7.0 and 7.4.

Glucose Measurement and Cell Concentrations

Glucose concentration was measured with a Yellow Springs Instrument Model 2700 Select Analyzer (YSI glucose membrane kit 2365, Yellow Springs, OH). Cell concentrations were determined by counting trypsinized cells with a hemocytometer. Spheroids were disassociated into single cells by first removing the cell suspension from the overlay plate and centrifuging at 100*g* for 1 min to remove the medium. The pellet was then suspended and gently mixed in preheated EBSS (Sigma, St. Louis, MO) containing 0.25% trypsin. Light microscopy was used to monitor the mixture for spheroid dissociation and membrane blebbing as an early indicator of membrane rupture. Dissociation of DU 145 spheroids normally occurred within 3 min, during which blebbing of single cells was minimal. The suspension was immediately centrifuged at 75*g* for 45 s to remove trypsin and the pellet resuspended in trypsin-free EBSS. Cell concentrations were then determined as described above.

Spheroid Distribution and Concentrations

Spheroid-size distributions and concentrations were determined with an Olympus IX 50 inverted light microscope and Image-Pro Plus analysis software (Media Cybernetics, Silver Spring, MD). Images were captured directly from the microscope by an Optronics digital camera, DEI-750 (C^2 Corp, Orlando, FL). For each time period 300 visual fields of 0.275 mm^2 were examined. This resulted in the analysis of 14,000 to 36,000 individual spheroids for each period. The visual fields were randomly selected from three or more liquid-overlay plates in duplicate experiments.

Based on protocols developed by Stokes et al. (1991), time-lapse images were digitally captured to estimate parameters such as cell self-diffusivity and collision frequency. Liquid-overlay plates were placed on a heated microscope stage at 37°C and covered with a glass incubator (Custom Medical Applications, Bally, PA). A stream of prehumidified medical-grade gas containing 5% CO_2 and 5% O_2 in N_2 was fed to the incubator at a rate of ~13 mL/h. Images were captured every 5 min for 24 h from four separate cultures.

Average Cell Number/Projected Spheroid Area Correlation

To determine the correlation between spheroid size and cell number, liquid-overlay cultures of DU 145 spheroids were first sieved through monofilament nylon mesh (Small Parts Inc., Miami Lakes, FL) with pore sizes ranging from 20 μm to 120 μm based on a protocol by Wigle et al., 1983. The nylon mesh was placed in 37-mm diameter styrene-acrylonitrile holders (Osmonics, Livermore, CA) with a stainless steel mesh support, pore-size 180 μm (Small Parts, Inc.). A chain of 4- to 5-mesh sizes, with a prefilter, was typically used to separate a number of spheroid sizes simultaneously. Individual filters were removed and washed in 1.5 mL of culture media. Using procedures described above, half of the resulting suspension was taken for determination of cell concentration while the remainder was analyzed for

spheroid size. Two spheroid classes were used to correlate spheroid size to cell number: early (those formed within the first 24 h of culture) and late (allowed to develop for at least 48 h).

Computer Simulation of Initial Clustering

Cell-cluster formation resulting from randomly distributed cells on a surface was investigated using a two-dimensional model based on the starting point of an off-lattice Monte-Carlo simulation. For the starting concentration of 2×10^4 cells/cm^2, 200 "cells," circles with radius 8.5 μm, were randomly distributed in a square 1000 μm × 1000 μm with periodic boundary conditions (Kolb, 1984; Meakin, 1985). Two differing distribution conditions were considered—one allowing neighbor overlap, and the other prohibiting overlap. A cluster boundary was then defined as the maximum distance at which two cells would be considered one cluster. Each cell could be assigned to only one cluster. Results were averaged over 200 simulations for each distribution and cluster boundary.

Kinetic Modeling

The coupled differential equations of the kinetic models were solved by numerical integration in Microsoft Excel using the Euler method with a 0.05-h time step. The kinetic-rate constants were determined by least-squares fitting of predicted model results to experimental data. The merit function to be minimized was the sum of the normalized, squared residual error between the predicted and experimental values of aggregate concentration.

Statistical Analysis

Spheroid-size distribution data were analyzed by repeated measures of analysis of variance followed by the Tukey A range test (BMDP Statistical Software, Inc., Los Angeles, CA). Spheroid adhesion probabilities were analyzed by chi-squared variance (BMDP Statistical Software, Inc.). A 0.01 level of probability was used as the criterion of significance. All values are reported as mean ± standard deviation for duplicate cultures.

RESULTS

Overview of Spheroid Development

The spheroid development of DU 145 cells in liquid-overlay culture was monitored with light microscopy over 18 d. The measurable parameter of spheroid size was the projection of a three-dimensional structure onto a two-dimensional surface, a projected area. During this period the average projected area per spheroid increased from 335 μm^2 to over 9500 μm^2, corresponding to an increase in average diameter of 20 μm to 110 μm (Fig. 1A). The spheroid development

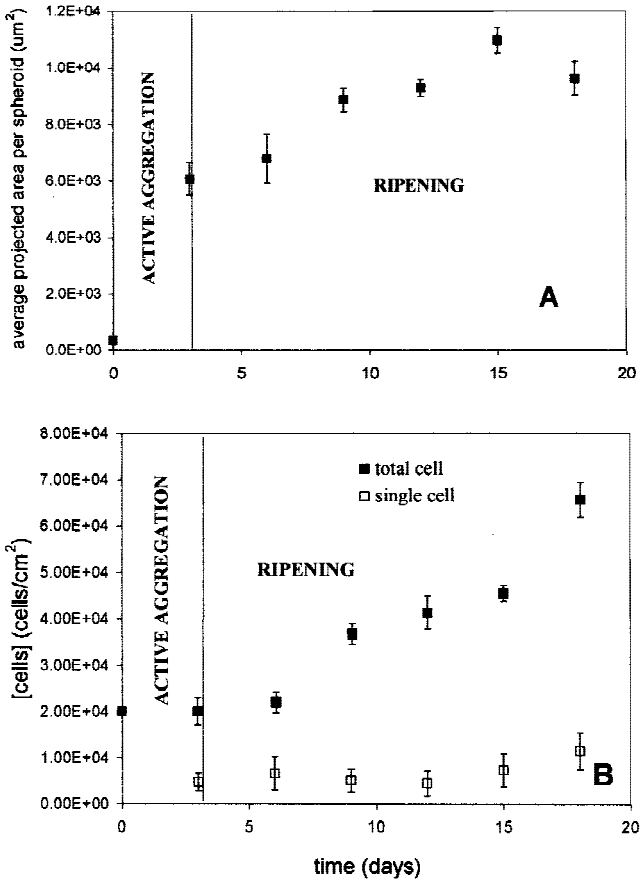

Figure 1. Growth characteristics of DU 145 human prostate cancer cells in liquid-overlay culture: (A) average projected area per spheroid, (B) total and single cell concentration vs. time. The transition between two distinct phases of aggregation has been indicated as mentioned in the Discussion section.

appeared to be biphasic with over 61% of the increase in spheroid size occurring within the first 3 days of culture—the lag phase of cellular growth (Fig. 1B). This rapid assembly of spheroids was followed by a much slower, sustained increase in size over the remaining 15 days during which the concentration of single cells remained constant. In this phase, total cell concentrations increased only threefold: a specific growth rate 1/10th of that published by our lab for DU 145 cells in monolayer culture (Clejan et al., 1996). This apparent reduction in cellular growth rate is, however, typical of the ripening phase in spheroidal systems where only the outermost cell layers proliferate (Donaldson et al., 1990; Yuhas and Li, 1978). The initial rapid increase in spheroid size was then not a function of internal cellular growth, but entirely due to coalescence among free cells and aggregates during the first 72 h of culture. The remaining experiments focussed on this initial development period.

Initial Clustering and Redistribution

Due to individual culture variation and the choice of imaging area, starting cell concentrations appeared greater than

the inoculum level. The starting cell concentration was empirically found to be $3.0 \pm .5 \times 10^4$ cells/cm^2. Although composed primarily of single cells, 23% of the spheroids in the culture inoculum were significantly larger than single cells at time = 0. These aggregations were at best only loose associations, as random cell movements created a rapid disaggregation within the first hour following culture inoculation (Fig. 2). Single-cell concentration increased slightly by a factor of 1.15, and the concentration of other existing aggregations decreased by factors of 0.36 to 0.69. These loose associations are defined hereafter as "clusters," while spheroids formed during active aggregation are "aggregates."

A computer simulation was developed to investigate if a random distribution of cells over the agar surface at the given cell density could have contributed to the initial clustering in our system. A representative diagram of the simulated distribution is shown in Figure 3A. The total cluster concentration derived solely from the random distribution of cells was determined by averaging over 200 simulations and plotted as a function of cluster boundary as defined in the Methods section (Fig. 3B). The estimated total cluster concentration initially increased with the cluster boundary parameter, reaching a maximum of 4.46×10^3 spheroids/cm^2 at boundary of 24 μm (the approximate equivalent of one cell diameter) for the condition of cell overlap. Allowing cell overlap, the experimental cluster concentration of $4.28 \pm 0.36 \times 10^3$ spheroids/cm^2 was reached with a boundary of only 9 μm beyond the cell radius; without cell overlap, the experimental concentration was reached with a boundary of at least 16 μm. Additionally, the predicted cluster-size distribution for both cases compares favorably to experimental values (Fig. 3C). A random distribution of single cells can, therefore, generate the distribution of clusters seen in our inoculum.

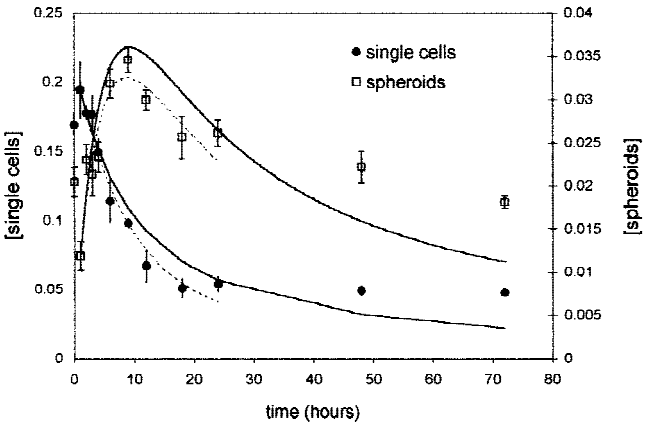

Figure 2. Concentration profiles of single cells and spheroids of DU 145 cells in liquid-overlay culture. The latter represents a lumped class of spheroids of all sizes. Dimensionless concentrations for single cells are given by the left ordinate and those for spheroids on the right ordinate. Solid lines represent model predictions integrating over 72 h; dashed lines represent integration over 24 h.

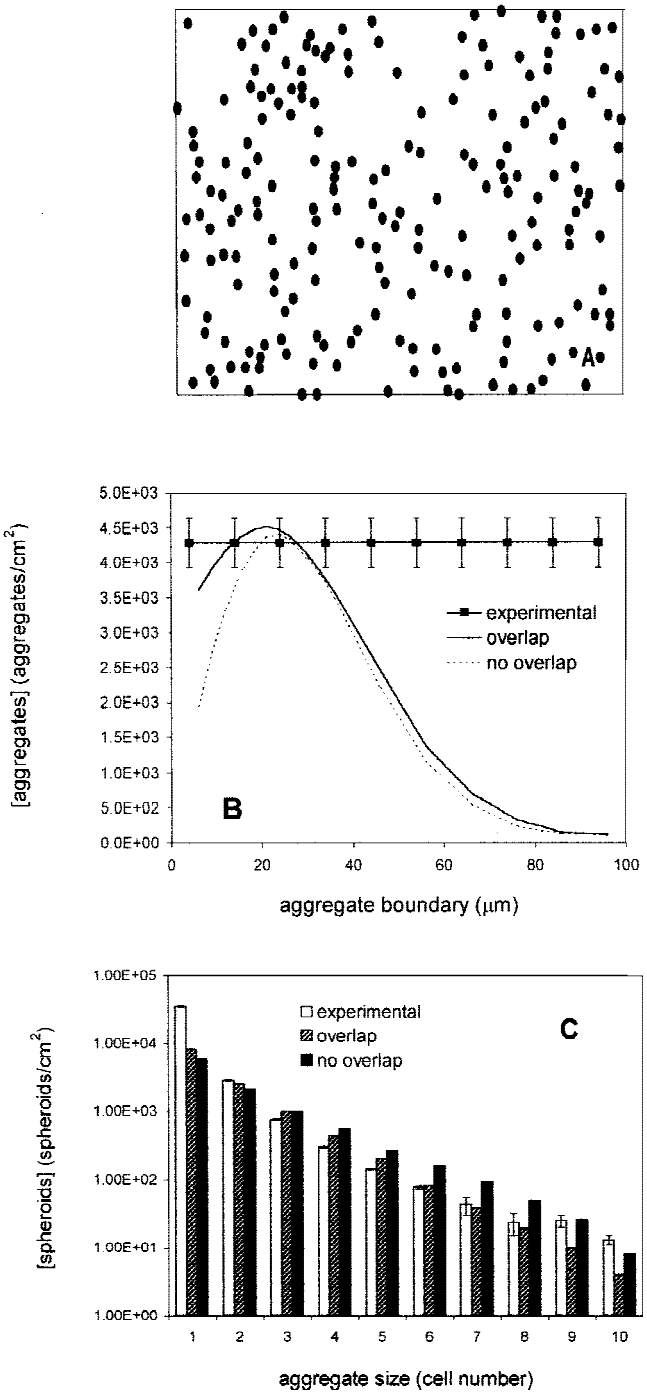

Figure 3. Simulation of initial aggregation patterns for DU 145 cells in liquid-overlay culture. Simulations are based on the starting concentration of 2×10^4 cells/cm^2, with an average cell radius of 8.5 μm using the random spatial distribution of 200 cells in a square 1000-μm wide with periodic boundary conditions. (A) Representative diagram for the condition of cell overlap. (B) Observed and predicted spheroid concentration (excluding single cells) at $t = 0$. (C) Initial cluster distributions corresponding to a cluster boundary of 9 μm beyond the cell radius for the condition of cell overlap and 16 μm beyond the cell radius for the condition of no cell overlap.

Active Spheroid Self-Assembly

Following conventions of surface aggregation science, spheroid size was defined in terms of monomer increments.

Projected spheroid area, A_{proj}, was converted to cell number, n, by the empirical correlation shown in Figure 4:

$$A_{proj}(\mu m^2) = 477.2 \cdot n^{2/3} \quad (1)$$

Both newly formed (18 h) and established (66 h) spheroids exhibited similar functionalities, indicating that spheroid compaction was negligible during this period. Equation (1) is consistent with the functionality predicted by spheroid geometry; however, the proportionality factor of 477.2 μm^2 is greater than the value predicted from the average cross-sectional area of a single cell— 227 μm^2. This discrepancy suggests that individual DU 145 cells did not retain a constant volume or uniform packing during aggregation, that spheroids were not perfect spheres, or that a combination of the two conditions existed. Equation (1) overestimates the projected area of single cells and small aggregates, but increases in fidelity with increasing cell number.

Spheroid formation as a function of time was determined by tracking concentration changes in multiple spheroid sizes over 72 h. The size distributions for all time periods were significantly different from each other ($p < 0.001$). Also as defined by surface science, concentrations were expressed as a dimensionless number density: spheroid concentration (spheroids/μm^2) per monomer unit area (μm^2), where single cells were considered spheroids of size = 1. The dimensionless density, spheroids/monomer, eliminates cell-size dependence from any developed mathematical model and allows for direct comparisons of kinetic constants from diverse systems. In this convention the monomer unit area was equal to 477.2 μm^2, and a concentration of 1×10^4 cells/cm^2 became 0.0477.

Following the transient redistribution, DU 145 cells in liquid-overlay culture exhibited a 24-h period of intense activity after which aggregation appeared to plateau (Fig. 5). During active aggregation, single-cell concentration decreased from 0.169 to 0.054, or 68%. Correspondingly, the concentration of dimers initially increased by a factor of 1.9 from 0.008 to a maximum of 0.017 at 9 h, followed by a steady decline to 0.012 at 24 h. Larger spheroids exhibited similar behavior, although the magnitude and occurrence of the maximum depended on spheroid size.

Although clusters containing more than 20 cells were observed at inoculation, following the transient redistribution, spheroids of this size remained undetectable until hours 2 or 3. These larger spheroids became increasingly scarce with increasing spheroid size, with the concentration of 30-mers at its maximum only 0.01% of the corresponding

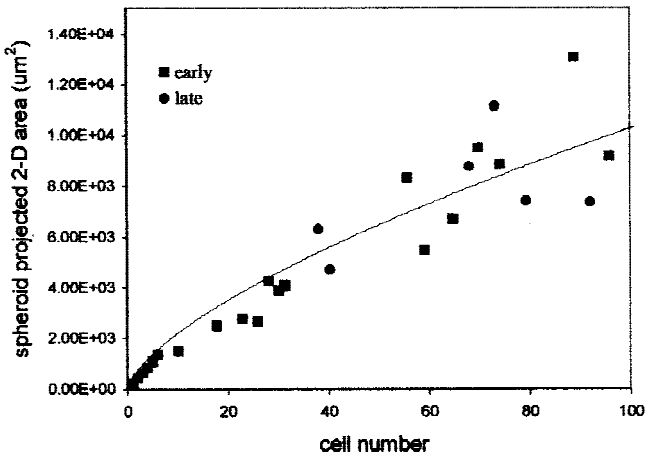

Figure 4. Average projected spheroid area, A_{proj}, vs. average cell number, n, within spheroids. Data were taken from separate cultures 18 h (early) and 66 h (late) after inoculation and weighted according to the number of samples in each size range. Plot includes the least-squares fit to data, $A_{proj} = 477.2 \cdot n^{2/3}$.

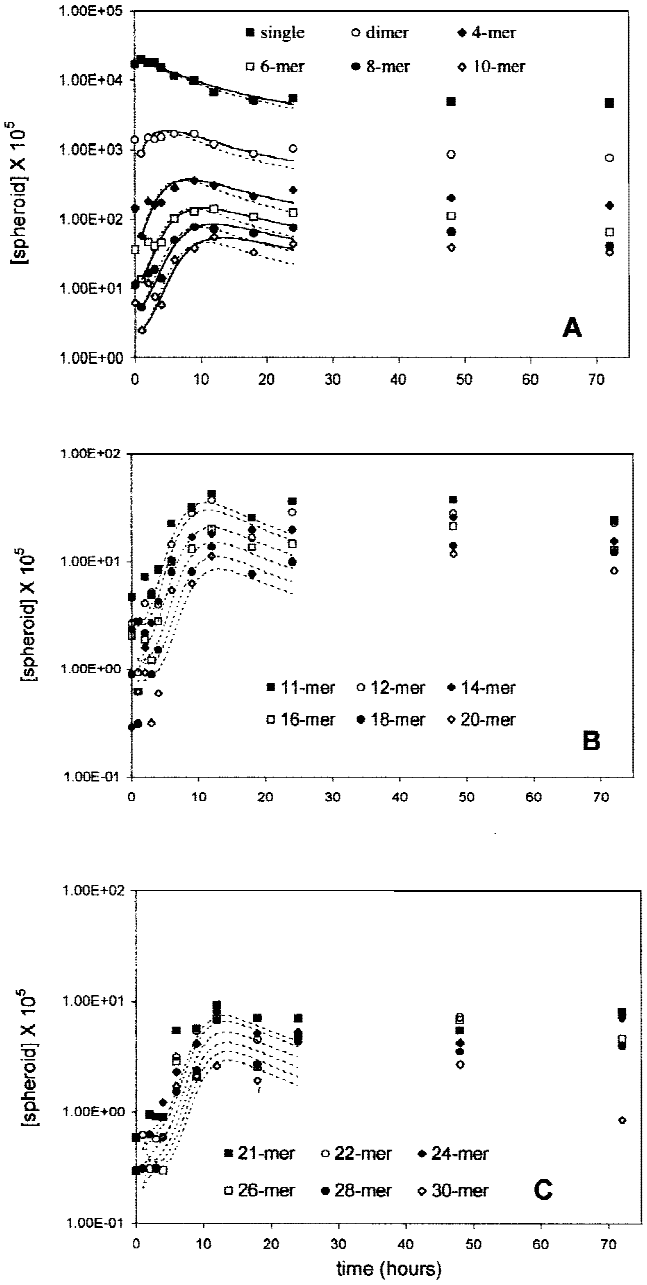

Figure 5. Concentration profiles of multiple-aggregate-size classes over time: (A) single cells–10-mer, (B) 11-mer–20-mer, and (C) 21-mer–30-mer. Model predictions for each class were determined by numerical integration over 24 h and are presented as solid lines for $i_{max} = 11$ and dashed lines for $i_{max} = 31$.

monomer concentration. The individual concentrations of spheroids containing more than 30 cells represented on average less than 2 in 50,000 counted spheroids and were subsequently summed into a single lumped class.

Kinetic Modeling of Aggregation

Based on Smoluchowski's coagulation theory (Smoluchowski, 1917), a set of coupled differential equations was developed to represent spheroid self-assembly:

$$\frac{dC_i}{dt} = 0.5\sum_{j=1}^{i-1} C_j C_{i-j} k_{j,i-j}(1+\delta_{j,i-j}) - C_i \sum_{j=1}^{i\ max} C_j k_{ji}(1+\delta_{ji}) \qquad i < i_{max} \quad (2)$$

$$\frac{dC_{i\ max}}{dt} = 0.5 \sum_{j=1}^{i\ max-1} \sum_{i=i\ max-j}^{i\ max-1} C_j C_i k_{j,i}(1+\delta_{j,i}) - C_{i\ max}^2\, k_{i\ max,\, i\ max} \qquad i = i_{max} \quad (3)$$

where C_i is the concentration of spheroids of size $= i$, k_{ij} is the rate of attachment of an object of size i to one of size j, t is the time, and i_{max} is the largest size class explicitly considered (aggregates of size $i > i_{max}$ are lumped into i_{max}). To satisfy the overall mass balance of the system, the first term is divided by 2 to avoid double-counting. The Kronecker delta, δ, accounts for collisions between spheroids of the same-size class. Equation (2) represents the net concentration of a particular spheroid size class i as a balance between their creation from spheroids of size j and $i-j$ and their depletion due to interactions with those of size j (all other sizes). For the smallest size class, $i = 1$, equation (2) is comprised only of the subtractive terms. Additionally, equation (3) is used as a special form of equation (2) for the final lumped class of the largest spheroids, $i = i_{max}$. As the model describes aggregation only during the lag phase of DU 145 culture (Fig. 1B), cellular-growth terms were not included. With the exception of the transient behavior at inoculation, disaggregation was not apparent in our liquid-overlay cultures with video microscopy and, as such, was not included in the model. The kinetic-rate-parameter constants were determined by numerical integration of model equations followed by a least squares fitting of predicted to experimental results. Boundary conditions were the experimental concentrations of spheroids at time $t = 1$ h, after the transient behavior.

Three differing models were developed that varied in their computational complexity by the degree to which spheroid size was resolved. The initial model defined only single cells and spheroids, $i_{max} = 2$, and focused on the contribution of single cells to the aggregation mechanism. This system allowed the independent rate coefficients to be explicitly determined. The intermediate test case, $i_{max} = 11$, was the largest system for which a solution was possible when all rate coefficients were varied independently and, as such, served to test various assumptions for reducing the number of variables in our model. The final case considered, $i_{max} = 31$, represents the upper-size limit for DU 145 spheroids in liquid-overlay culture as previously described in this section.

The initial model results, $i_{max} = 2$, presented in Figure 2 as solid lines adequately represent experimental trends, especially during the first 24 h. For the 48-h plateau period, however, the model overestimates both single-cell and spheroid depletion. Model predictions for the most active period of spheroid self-assembly were improved to within experimental error by limiting integration to the initial 24 h (Fig. 2, dashed lines). This resulted in a decrease in the error function for the 24-h period of 61%. Constant kinetic rate parameters were, therefore, applicable only during the initial 24 h, suggesting a possible change in aggregation mechanisms after this time. The improved fit corresponded to rate constants $k_{11} = 0.20\ h^{-1}$, $k_{SS} = 1.82\ h^{-1}$ and $k_{1S} = 1.17\ h^{-1}$ (approximately the average of k_{11} and k_{SS}), where subscript S denotes all spheroids. These values indicate that successful cell–spheroid and spheroid–spheroid interactions dominate the aggregation process, occurring at least 6 times faster than cell–cell interactions.

In general, there are $0.5(i_{max})(i_{max}+1)$ independent-rate constants in our model, because $k_{ij} = k_{ji}$. For $i_{max} > 2$, we tested various assumptions for further reducing the number of independent variables to facilitate solution of model equations and physical interpretation of model results. First, we represented the diagonal rate constants with a polynomial in i and determined the order of this expression that generated the best model fit to our aggregation data. In this analysis, the solution for a given polynomial served as the initial guess of rate constants for the next higher order. Based on results from the $i_{max} = 2$ model, fits were compared for the cases when off diagonal rate constants were approximated as the arithmetic and geometric mean of the corresponding diagonal values.

The test case, $i_{max} = 11$, showed a first-order estimate of diagonal rate constants ($k_{ii} = 1.96(i) - 1.75\ h^{-1}$) reduced the residual error by nearly 90% over the model fit obtained for constant k (Table I). The fit shown in Figure 5 as the solid line was not significantly improved by further increasing the degree of freedom of the polynomial estimate to the case where all 11 diagonal values were independent. Further reductions in model error required significant increases in the degree of freedom: the limiting case of 66 independent parameters resulted in a further reduction of only 20%. For all forms considered, comparable model fits were obtained with off-diagonal k's defined as either arithmetic or geometric averages (Table I). Similar results were obtained when the model was expanded to describe monomers through 30-mers. Both models predict values of k_{ii} as increasing with spheroid size and provide excellent fits to the experimental data (Fig. 5). Unlike the $i_{max} = 11$ case, model fits for $i_{max} = 31$ were slightly improved with a third-order estimate of diagonal rate constants ($k_{ii} = 0.01(i)^3 - 0.20(i)^2 + 2.94(i) - 2.51\ h^{-1}$) and off-diagonal k's

Table I. Total squared error for predictions of spheroid aggregation, $i_{max} = 11$ and $i_{max} = 31$ models.

Number of independent parameters	Estimation of k_{ii} (h^{-1})[a]	Total squared error/data point × 10^2	
		$i_{max} = 11$	$i_{max} = 31$
1	$k_{ii} = 0.330$[b] $k_{ii} = 0.335$[c]	60.81	79.38
2	$k_{ii} = 1.96(i) - 1.75$[b,d] $k_{ii} = 3.30(i) - 3.17$[c,e]	7.564[e] 6.427[d]	42.11[e] 48.60[d]
3	$k_{ii} = 0.02(i)^2 + 1.84(i) - 1.64$[b,d] $k_{ii} = 0.14(i)^2 + 1.21(i) - 1.08$[c,e]	7.556[e] 6.349[d]	39.12[e] 45.73[d]
4	$k_{ii} = -0.01(i)^3 + 0.08(i)^2 + 1.64(i) - 1.50$[b,d] $k_{ii} = 0.01(i)^3 - 0.20(i)^2 + 2.94(i) - 2.51$[c,e]	7.553[e] 6.336[d]	38.34[e] 44.36[d]
5	$k_{ii} = 0.001(i)^4 - 0.01(i)^3 - 0.10(i)^2 + 1.89(i) - 1.73$[c,e]		38.26[e] n/a[d]
11	independent over $i = j$	6.716[e] 6.202[d]	
66	independent over all i,j	4.872	

[a]Expression parameters determined by numerical integration over 24 h and least squares analysis of predicted and experimental results. Boundary conditions determined from experimental spheroid concentrations at 1 h.
[b]Estimation for $i_{max} = 11$.
[c]Estimation for $i_{max} = 31$.
[d]Values calculated with k_{ij} as the arithmetic average of k_{ii} and k_{jj}.
[e]Values calculated with k_{ij} as the geometric average of k_{ii} and k_{jj}.

defined as the geometric average (Table I). Both diagonal estimates are also in agreement with the lumped-model solutions where $k_{11} < k_{SS}$. The consistent results for the three i_{max} cases and the similar fits predicted using either a geometric or arithmetic definition of k_{ij} imply results that are not artifacts of the specific approximations.

Factors Determining Rate Constants

The physical mechanisms governing biological aggregation have traditionally been evaluated based on theories first proposed by Smoluchowski (1917). His rate expression for an elementary, nonionic, diffusion-controlled reaction is

$$k_{ij} = \beta_{ij}(R_i + R_j)(D_i + D_j) \quad (4)$$

where β is the proportionality constant, R_i the radius of influence, and D_i the self-diffusion coefficient of a spheroid of size *i*. The equation is valid for the aggregation of perfect spheres in a dilute solution undergoing Brownian motion. Smoluchowski defined β_{ij} as equal to $4\pi N_a$, where Avagadro's constant, N_a, accounts for molecular reactions and as such is invalid for our system. The constant also assumes that the probability of adhesion following contact is constant and near 100%. The sum $(R_i + R_j)$ represents the radius of influence of aggregation: the maximum distance between the centers of spheroids size *i* and *j* at which aggregation can occur. For perfect spheres R_i is equal to the radius of the spheroid, r_i. For Brownian motion in a dilute solution, the diffusion coefficient D_i is inversely proportional to r_i (Rowley, 1994). Using these assumptions the definition of k_{ij} becomes:

$$k_{ij} = \beta_{ij}\frac{(r_i + r_j)^2}{(r_i r_j)} \quad (5)$$

where β_{ij} represents a constant adhesion probability combined with the proportionality factor between diffusivity and spheroid radius, here used as the single-fitting parameter. The best-fit model solution using Equation (5) results in a residual error per data point of 60.7 for $i_{max} = 11$ and 79.3 for $i_{max} = 31$ (Table II), both equivalent to the respective mathematical solutions using constant *k* (Table I). This poor fit prompted an investigation into the discrepancies between the self-assembly of DU 145 spheroids and aggregation in Smoluchowski's idealized system.

In liquid-overlay culture, it is generally assumed that cell motility on the nonadherent agar surface is limited and described by Brownian-type behavior (Yuhas et al., 1977). In contrast, time-lapse video microscopy revealed that our liquid-overlay cultures exhibited initially high levels of motility lasting at least 5 h, followed by a gradual decrease as larger spheroids were formed (Fig. 6: animations may be viewed at http://www.tulane.edu/~kim/animation.html). Control cultures of nonviable DU 145 cells failed to exhibit movement of any kind, indicating that the observed cellular motion was purely a biological process (data not shown).

Table II. Total squared error for predictions of spheroid aggregation, Smoluchowski-rate expression.

Alteration from ideal	Total squared error/data point × 10^2	
	$i_{max} = 11$	$i_{max} = 31$
None	60.73	79.32
Diffusivity	63.04	79.93
Adhesion probability	46.10	72.34
Linear estimation of β	6.41	49.43
Radius of influence	60.19	79.12

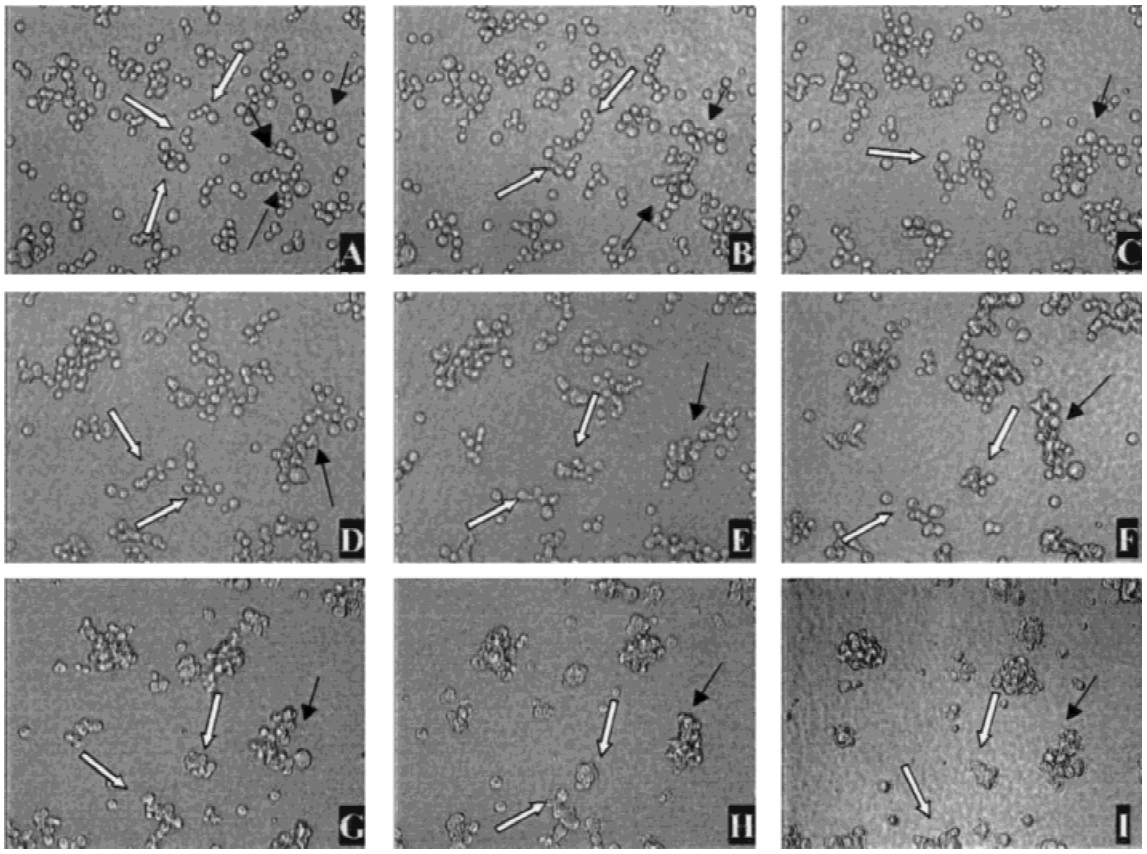

Figure 6. Time-lapse images of DU 145 cells aggregating into spheroids in liquid-overlay culture. A: 1 h; B: 1 h 20 min; C: 1 h 40 min; D: 2 h 30 min; E: 3 h 20 min; F: 5 h; G: 8 h 30 min; H: 10 h; I: 16 h. Black arrows follow branched structures that aggregate to form a single spheroid. White arrows indicate similar structures that collide yet do not aggregate.

The self-diffusion coefficient, D, was calculated by the Einstein relation (Rowley, 1994):

$$D = \lim_{t\to\infty} \frac{\langle R(t)^2 \rangle}{2dt} \tag{6}$$

where d is the dimensionality of the system (2 for liquid-overlay cultures) and $\langle R(t)^2 \rangle$ is the mean-square displacement of the spheroid at time t. To maximize the use of data, the displacements were calculated from independent nested time loops: at 0 and 6 h, 1 and 7 h, 2 and 8 h, etc. Results are shown in Figure 7. The diffusion of single cells was 6 times faster than either dimers or trimers and 37 times faster than spheroids containing more than 10 cells. The Brownian assumption, $D_i \propto r_i^{-1}$, approximates the diffusivity for larger spheroids (solid line, Fig. 7), but is unable to account for the increased activity observed in dimers, trimers, and especially single cells. By allowing the function to become discontinuous at monomers and fitting the remainder of the data to a power law ($D_i \propto r_i^x$), the total squared error between predicted and experimental diffusivities was improved by 80% (dashed line, Fig. 7). However, when the improved functionality was substituted for Brownian diffusion in the Smoluchowski expression, the resulting residual error of the model slightly increased: by 1% for $i_{max} = 11$ model and <1 % for $i_{max} = 31$ (Table II). The diffusive properties of the system minimally impact the resulting rate expression, suggesting that aggregation in the liquid-overlay system is governed by other mechanisms.

Nonideal behavior was similarly noted in the adhesion probabilities of DU 145 spheroids in liquid-overlay culture. Adhesion probability was measured by tracking spheroid

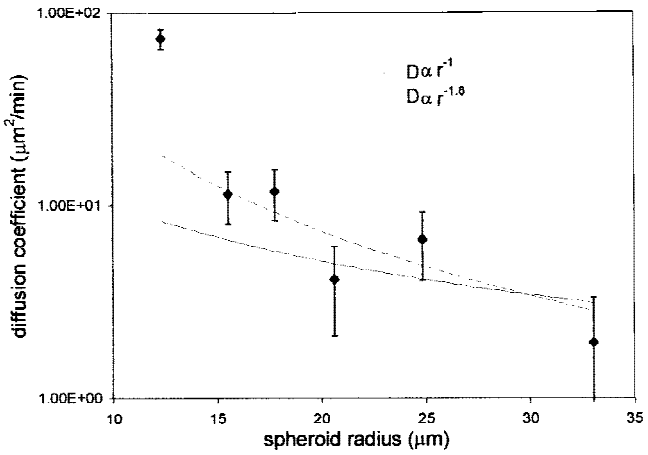

Figure 7. Self-diffusion coefficients for spheroids (including single cells) as determined by Einstein's relation and Brownian assumptions from time-lapse images of DU 145 liquid-overlay cultures. Plot includes least-squares fit using either a Brownian (solid line) or discontinuous for monomers (dashed-line) functionality.

collisions for successful and nonsuccessful aggregations in multiple-size classes. The probability of adhesion was found to be spheroid-size dependent, and no class exhibited 100% successful aggregation on collision. For all aggregation events in our system, profound morphological changes accompanied spheroid coalescence. The most visible and distinguishable marker for successful aggregation was the blurring of individual spheroid boundaries—used as the general indicator of aggregation in our system (Fig. 6G–I; Fig. 8C). For purposes of statistical significance three classes of collision were defined: cell–cell, cell–spheroid, and spheroid–spheroid, where a spheroid contains three or more cells (Table III, $p < 0.01$). The most efficient collisions were between single cells and larger spheroids, producing successful aggregations 83% of the time, twice as often as collisions between established spheroids and 5 times more often than interactions between individual DU 145 cells. Although written for a diffusion-controlled reaction, Smoluchowski's expression can be altered to account for changes in adhesion by allowing β to vary with spheroid size. Model fit was improved by 25% for $i_{max} = 11$ and 10% for $i_{max} = 31$ by the inclusion of the determined adhesion probabilities alone (Table II). For both $i_{max} = 11$ and $i_{max} = 31$, this fit was further improved to agree with previous best-fit mathematical solutions (Table I) by allowing β to linearly increase with spheroid size (Table II).

Image analysis revealed that the experimental radius of

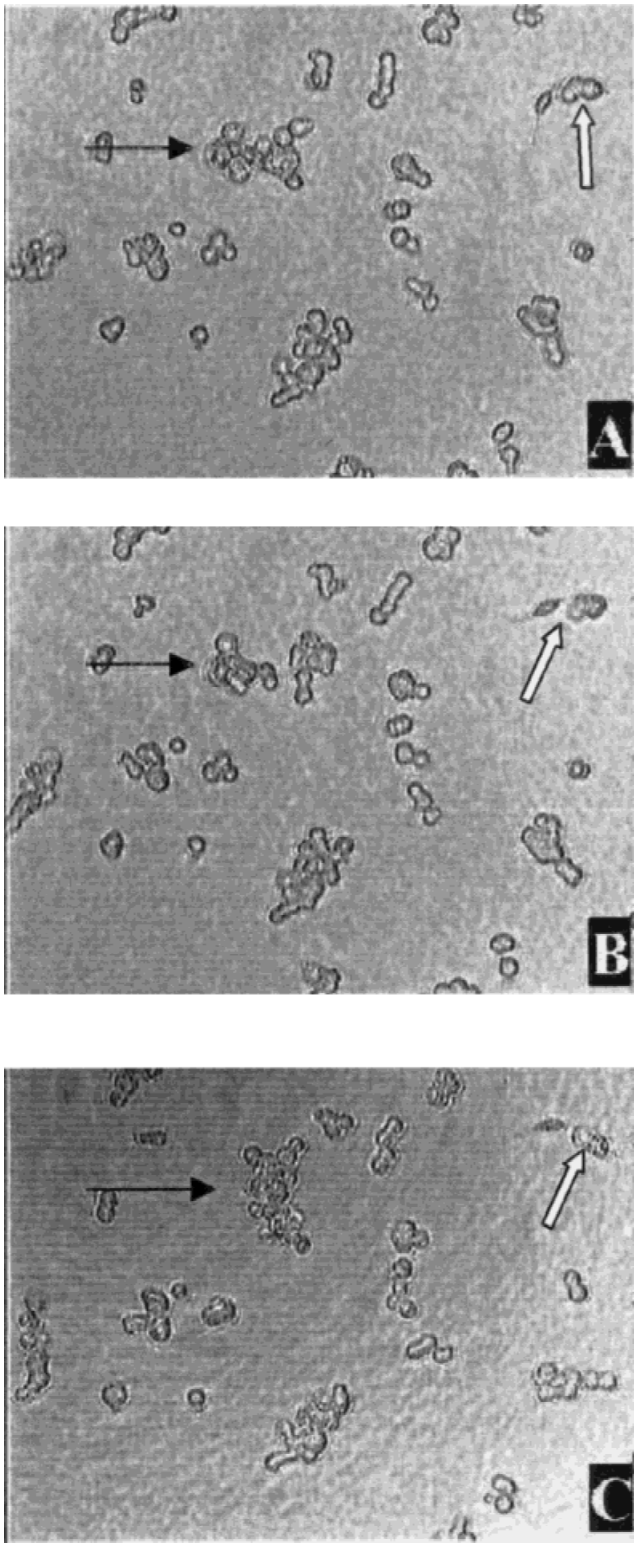

Figure 8. Examples of "orbiting" (black arrows) and "tethering" (white arrows) behavior in time-lapse images of DU 145 cells in liquid-overlay culture. A: 3 h; B: 3 h 10 min; C: 3 h 55 min.

Table III. Aggregation parameters from time-lapse photography.

Class of interaction	% of successful collisions
Cell–cell	16.6 ± 4.1[a]
Cell–spheroid[b]	83.1 ± 9.1[c]
Dimer–dimer	40.0 ± 6.7[d]
Dimer–spheroid	52.4 ± 6.7[d]
Trimer–trimer	n/a
Trimer–spheroid	33.3 ± 6.7[d]
Spheroid–spheroid	55.6 ± 6.7[d]

[a,c,d]Indicates statistically significant groups.

[b]For purposes of this table, a spheroid is defined as containing more than three cells.

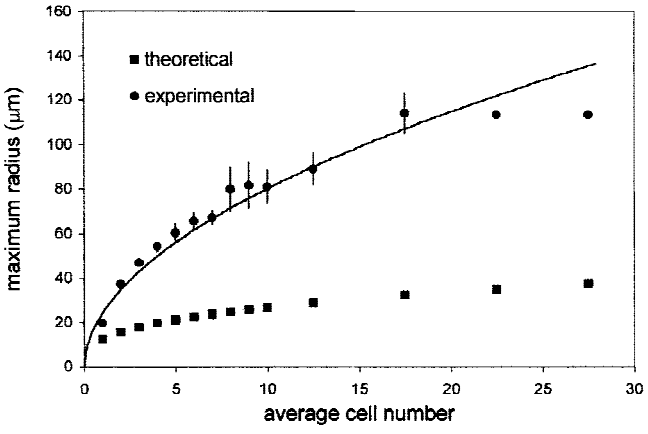

Figure 9. Comparison of experimental and theoretical average-maximum radius, *R*, of a spheroid as a function of spheroid cell number, *n*. Theoretical values are based on perfect spherical geometry. Plot includes the least-squares fit of experimental data, $R = 24.2 \cdot n^{0.51}$.

influence, R, was larger than the theoretical estimates based on spherical geometry. Aggregates were rarely symmetrical, especially at early time periods where their structure was primarily oblong or branched (Fig. 6A–F). Such structures would tend to "sweep" an area much larger than that predicted by the average radius. A better estimate of their effective radius of influence was hypothesized to be the maximum radius of the aggregate. Using the correlation in Figure 4, the maximum radius (R_m) was plotted as a function of cell number (n) and compared to the theoretical values assuming perfect spheres (Fig. 9). While the experimental values were greater than those of the ideal case, the best-fit power laws of each resulted in similar functionalities—theoretical, $R_m \propto n^{0.33}$; experimental, $R_m \times n^{0.56}$—as well as similar results when introduced into the Smoluchowski expression. The experimentally determined function improved model fit by less than 1% over the theoretical (Table II), serving only to alter the factor β.

The possibility also exists that R should be further increased beyond the physical boundary of the spheroid due to attractive effects of chemotactic agents or membrane extensions. Examples of such forces are readily evident in the time-lapse video images of DU 145 aggregation. Spheroid–spheroid aggregations were often preceded by an "orbiting" period lasting from 30 to 60 min where the aggregates would closely circle one another rapidly coming together and moving apart (Fig. 8, black arrow). During this period contact between spheroids usually lasted 5 min or less. If the contact lasted longer than 20 min, the aggregation was permanent and no subsequent dissociation was observed. In contrast, single cells were found to employ active membrane extensions several cell-diameters long to reach toward a neighboring aggregate (Fig. 8, white arrow). Similar, but smaller, structures have also been observed in aggregating hepatocytes (Powers and Griffith-Cima, 1995). These smaller structures also appear in our system, but only when the aggregates lie very near one another and seem to operate only over relatively short distances. Both forms of intercellular communication are thought to be a means of anchorage for subsequent cell movement and attachment, "tethering" single cells and small aggregates to larger spheroids. (Examples of both forms of aggregation may be viewed at http://www.tulane.edu/~kim/animation.html.)

DISCUSSION

Over the past decade, the variety of three-dimensional prostate cultures has increased as a result of improved methods of cultivation (O'Connor, 1999). However, the mechanisms of formation in these cultures is ill-defined and many systems exclude significant portions of their cultures by sieving or selective sedimentation to better define starting conditions before experimentation. The excluded portions of the culture may, however, represent a clinically significant phenotype that would otherwise profoundly alter experimental findings. Using a single-cell suspension of DU 145 cells created from a trypsinized monolayer, we have characterized three distinct phases of spheroid development in liquid-overlay culture: a rapid redistribution of the initial aggregation pattern, an active self-assembly into spheroids described by constant rate coefficients, and a ripening phase of established spheroids characterized by much slower kinetics.

Redistribution of Initial Aggregation

Although the liquid-overlay inoculum is composed primarily of single cells, a highly nonuniform distribution of cluster size is observed at $t = 0$. Our computer simulations suggest that this initial pattern of aggregation is essentially a function of the cell density of the inoculum and can be described solely on the basis of random cell placement and overlap. The rapid reorganization into smaller spheroids prior to aggregation further suggests that they are merely clusters of single cells.

The transient nature of the redistribution phase suggests a period of adaptation to liquid-overlay culture before aggregation can proceed. Immediately after inoculation the cell movements appear totally random and unaffected by neighboring cells; additionally, cell–cell and cell–aggregate adhesions are minimal. Within 1 h these trends are reversed: cell movement becomes oriented to established spheroids, and cellular adhesions become prevalent. These active processes necessarily involve functional surface proteins. The adaptation period may then represent the time required for attachment to the agar substrate for directed cellular mobility. An alternate explanation for the transient trends is offered by Fröhlich theory. This postulates the existence of attractive forces in biological systems similar to coherent interactions known to exist between molecules (Fröhlich, 1980; Rowlands et al., 1981a). Fröhlich-type interactions are theorized to be short-range attractive forces dependent on cellular potential and have been found to greatly influence roleaux formation in human erythrocytes (Rowlands et al., 1981b). Acting over distances of approximately one-cell diameter, these attractive forces are disrupted or abolished by significant shifts in pH, metabolic energy depletion, or alterations of membrane structure. At the very least, the trypsin treatment to create a single-cell dispersion disrupts cell-adhesion molecules and other membrane proteins—theoretically disrupting these forces and allowing for the random redistribution at culture initiation. However, as the integrity and structure of the membrane is reestablished, Fröhlich forces resume causing the cells to associate.

Spheroid Self-Assembly

The most active period of aggregation occurred immediately following the transit redistribution and lasted nearly 24 h. The physical assumptions governing such uniform coagulating systems have traditionally been described using Smoluchowski theory (Hardy and Beck, 1986; Samsel and Perelson, 1984). This defines the rate coefficient in a diffusion-controlled system as a function of three param-

eters based on size: the spheroid diffusivity, adhesion probability, and radius of influence. Comparison of the expression with our model results indicates the primary assumption of a diffusion-controlled reaction is invalid for our system. In mathematical solutions, all our models point to a rate parameter matrix that increases along the diagonal with increasing spheroid size. Only the trends for adhesion probability and radius of influence are able to provide this functionality, suggesting that they are the dominant parameters in our system. These findings suggest that the aggregation mechanism in our system is primarily reaction controlled: that spheroid adhesion occurs much slower than spheroid collision.

This contradicts the typical findings in previous studies of homotypic cell aggregation; however, these systems use highly modified cultures of attachment-independent cell lines that are naturally nonadherent (Neelameghan et al., 1997; Rowlands et al., 1981a, 1981b). Experimental conditions were adjusted so that ideal assumptions in the Smoluchowski parameters are valid. Adhesion is mediated by introducing antibodies to the media to create unimodal surface antigen–antibody-surface antigen reactions, and thus is assumed constant. To better visualize the resulting aggregation, cell mobility is also often reduced by increasing media viscosity. This creates an ideal diffusion controlled system in which the antibody bridging is much faster than particle coalescence (Hart and Chak, 1980). These reactions are then governed by the diffusive properties of the particles.

Normally these diffusive properties are described by Brownian-like motion. This ideal assumption has been shown valid in multiple-cell systems and is again shown as describing the mobility of large DU 145 spheroids in liquid-overlay culture; however, significant deviations from ideal behavior were noted for single cells and smaller aggregates. For this size range, the dramatic decrease in diffusivity with increasing size is consistent with our observation that DU 145 cells lose their ability upon aggregation to extend long tethers for mobility. These findings suggest a change in the cell surface perhaps as aggregates synthesize and surround themselves in extracellular matrix. The three-dimensional structure resulting from aggregation has been shown to be capable of up-regulating several matrix molecules including collagen IV and laminin in DU 145 cells (O'Connor et al., 1997).

Similarly, the ideal assumption of constant-adhesion probability is inapplicable to our system. The constant-adhesion probability in the systems mentioned above was determined primarily by surface-antigen density and antibody concentration. In our system, intercellular adhesion is more complex due to the multiple adhesion and matrix molecules expressed by attachment-dependent cells. Relative to spheroid–spheroid adhesion, single cells exhibit markedly reduced self-adhesion while adhesion to larger spheroids is dramatically increased. The profound shift in adhesion properties upon aggregation is consistent with the up-regulation of cell–cell and cell–cell-matrix bonds as seen in O'Connor et al. (1997)—events likely to activate cells into becoming more adhesion prone. An alternate explanation is that apparent increases in adhesion probability with spheroid size are simply due to the larger surface area presented to the culture and are therefore more a function of radius of influence. The two increasing functionalities, adhesion probability and radius of influence, are intertwined mathematically. Equivalent solutions and rate coefficients may be generated by either trend providing the dominant functionality or by a combination of both. The apparent dominance of the experimental adhesion probabilities in reducing model error may then be due, in part, to an underestimated radius of influence.

Intercellular attractive forces effectively extend the radius of influence beyond the physical boundaries of the spheroid. Both chemoattractive agents secreted by spheroids into the culture medium and shorter range Fröhlich-type interactions based on charge potential may stimulate directed motility in our culture system, possibly creating the orbiting and tethering behavior observed before most aggregations. Improvements to the ideal estimates of radius of influence are, however, limited to the visualized parameters in our system. The radius of a spheroid is typically determined by assuming spherical geometry and calculating the spheroid radius from the average projected area. This greatly underestimates the area "swept" by the branched or chained structures visible in our culture. As a correction, the maximum spheroid radius was hypothesized a better method of describing the radius of influence of a spheroid due to imperfect shape. Further increases to this functionality necessary to improve model fit may possibly be generated by the general inclusion of other visualized parameters such as active membrane extensions.

Ripening

Following the initial 24-h period of liquid-overlay culture, the spheroids enter a phase of development dominated by cellular growth. The trends predicted by the constant-rate coefficients begin to overestimate continued aggregation at this junction, suggesting an abrupt shift in reaction mechanism. During these later times, the absence of prominent increases in larger spheroid concentration together with the slow, steady increase in spheroid size suggests little spheroid–spheroid coalescence and only established spheroid growth controlled essentially by cellular division, or ripening. The control of spheroid development then shifts from inter- to intra-spheroid mechanisms. The observed decline in aggregation rates cannot be attributed to decreasing mobility with increasing spheroid size, as it affects all size classes within a short period of time. This pattern may be explained by either a profound decrease in the mobility or adhesion of the entire culture, or a combination of the two.

The absence of aggregation at later times may be generated by the differentiation of the outermost cell layers of the spheroids to nonadherent cell types. Spheroidal culture often results in cellular differentiation (Sutherland and Du-

rand, 1984) and could induce the partial expression of the columnar secretory phenotype from which the DU 145 line arose (Stone et al., 1978). This phenotype exhibits the typical epithelial polarized pattern of adhesion molecules. Only the basal layer and intercellular regions of epithelial cells in vivo issue present adhesion molecules, serving to anchor the cell to the underlying basement membrane and, through desmosomes, create a tight-fitting cell sheet that functions primarily as a molecular barrier (Alberts et al., 1994). The exposed surface of the cell can be absorptive, secretory, or ciliated, but all resist many forms of biological adhesion. Although not seen in monolayer cultures, this polarity has been reestablished in epithelial-cancer lines through low-shear spheroidal culture (Pervez et al., 1989). In quiescent environments multicellular aggregates of DU 145 cells exhibit a differentiated morphology through the expression of filopodia and microvilli-like structures (Clejan et al., 1996). The differentiated DU 145 spheroids would likely resist further adhesion to either single cells or other spheroids.

Applications

Two of the most promising applications of spheroid culture have been traditionally in vitro drug/therapy testing and more recently, tissue regeneration. With respect to the latter, bioartificial liver devices currently entrap hepatocytes within a collagen matrix; however, when cultured as spheroids, hepatocytes display enhanced liver-specific functions and, as such, may reduce scale-up requirements and enhance device performance (Lazar et al., 1995). Spheroidal culture is used routinely to induce stem-cell differentiation. For mouse embryoid bodies, or spheroids of embryonic stem cells, differentiation parallels the development of post-implantation embryos (Sauer et al., 1998). In vitro testing of anti-cancer agents using spheroidal cultures has revealed the mechanisms of chemo-resistance observed in many in vivo tumors as well as methods to combat it. Estramustine was found not to be subject to the conventional penetration barriers many therapeutic agents experience, instead preferentially binding to the degenerative cells at the spheroid core. It increased the relative extracellular space in these regions, allowing for the possibility of greater drug penetration by a secondary agent (Essand et al., 1993). Our kinetic model should be useful in improving the fidelity of spheroid cultures for these existing applications by creating spheroids of greater surface area, enhanced viability, and within a defined size range. A potentially new application for spheroid culture is as an aggregation assay for metastatic potential that focuses on the initial stages of metastasis, cell shedding from the primary tumor, in which our model will provide a quantitative assessment of cell adhesion. The multiple versions of the model demonstrate its inherent flexibility, providing control over the computational complexity of the aggregation assay by selecting the extent of aggregate-size resolution.

CONCLUSIONS

The kinetic model developed begins to describe the dynamics affecting the self-aggregation of DU 145 cells in liquid-overlay culture. In its initial application, the model has demonstrated success on two fronts, as an aid to understanding the underlying physical mechanisms controlling aggregation in our system and as a quantitative tool for measuring the self-adhesive properties of DU 145 cells. Experimental results suggest that self-aggregation in our system is divided into three distinct phases: a transient reorganization of initial cell clusters, a rapid aggregation characterized by constant-rate coefficients, and a ripening phase of established spheroids. Comparison of reaction coefficients with model results indicate that the most active period of self-assembly in DU 145 cells is primarily reaction controlled: The dominant functionality is the probability of successful collision and to a lesser extent the radius of influence over which the cells aggregate. Possible applications of the model include improving spheroid fidelity for tissue regeneration and in vitro drug testing, and comparing the metastatic potential of different cell lines.

This work is dedicated to June R. Enmon.

References

Alberts B, Bray D, Lewis J, Raff M, Roberts K, Watson JD. 1994. Molecular biology of the cell, 3rd ed. New York: Garland Publishing, Inc. 951 p.

Becker JL, Prewett TL, Spaulding GF, Goodwin TJ. 1993. Three-dimensional growth and differentiation of ovarian tumor cell line in high aspect rotating-wall vessel: Morphologic and embryologic considerations. J Cell Biochem 51:283–289.

Clejan S, O'Connor KC, Cowger NL, Cheles MK, Haque S, Primavera AC. 1996. Effects of simulated microgravity on DU 145 human prostate carcinoma cells. Biotechnol Bioeng 50:587–597.

Donaldson JT, Tucker JA, Keane TE, Walther PJ, Webb KS. 1990. Characterization of human prostate cancer: The multicellular tumor spheroid. Int J Cancer 46:238–244.

Durand RE. 1990. Multicell spheroids as a model for cell kinetic studies. Cell Tissue Kinet 23:141–159.

Essand M, Nilsson S, Carlsson J. 1993. Growth of prostatic cancer cells, DU 145, as multicellular spheroids and effects of estramustine. Anticancer Res 13:1261–1268.

Fröhlich H. 1980. The biological effects of microwaves and related questions. Adv Electron Electron Phys 53:85–152.

Hardy CD, Beck JS. 1986. Coagulation in cell suspensions: extensions of the von Smoluchowski model. J Theor Biol 120:181–189.

Hart HE, Chak KC. 1980. Theory of antigen-antibody induced particulate aggregation-I. General assumptions and basic theory. J Math Biol 42:17–36.

Kolb M. 1984. Unified description of static and dynamic scaling for kinetic cluster formation. Phys Rev Lett 53:1653–1656.

Lazar A, Peshwa MV, Wu FJ, Chi CM, Cerra FB, Hu WS. 1995. Formation of porcine hepatocyte spheroids for use in bioartificial liver. Cell Transplant 4:259–268.

Lelkes PI, Ramos E, Nikolaychik VV, Wankowski DM, Unsworth BR, Goodwin TJ. 1997. GTSF-2: A new, versatile cell culture medium for diverse normal and transformed mammalian cells. In Vitro Cell Dev Biol 33:344–451.

Meakin P. 1985. Off lattice simulations of cluster-cluster aggregation in dimensions 2-6. Phys Lett 107A:269–272.

Neelamegham S, Munn LL, Zygourakis K. 1997. A model for the kinetics of homotypic cellular aggregation under static conditions. Biophys J 72:51–64.

O'Connor KC, Enmon RM, Dotson RS, Primavera AC, Clejan S. 1997. Characterization of autocrine growth factors, their receptors and extracellular matrix present in three-dimensional cultures of DU 145 human prostate carcinoma cells grown in simulated microgravity. Tissue Eng 3:161–171.

O'Connor KC. 1999. Three-dimensional cultures of prostatic cells: Tissue models for the development of novel anti-cancer therapies. Pharm Res 16:486–493.

Pervez S, Kirkland SC, Epenetos AA, Mooi WJ, Evans DJ, Krausz T. 1989. Effect of polarity and differentiation on localization in multicellular tumor spheroid and xenograft models and its potential importance for in vivo immunotargeting. Int J Cancer 44:940–947.

Powers MJ, Griffith-Cima L. 1996. Motility behavior of hepatocytes on extracellular matrix substrata during aggregation. Biotechnol Bioeng 50:392–403.

Rowlands S, Sewchand LS, Lovlin RE, Beck JS, Enns EG. 1981a. A Fröhlich interaction of human erythrocytes. Phys Lett 82A:436–438.

Rowlands S, Sewchand LS, Enns EG. 1981b. Further evidence for a Fröhlich interaction of erythrocytes. Phys Lett 87A:256–260.

Rowley RL. 1994 Statistical mechanics for thermophysical property calculations. New Jersey: PTR Prentice Hall. 304 p.

Sacks PG, Oke V, Amos B, Vasey T, Lotan R. 1989. Modulation of growth, differentiation and glycoprotein synthesis by B-all-trans retinoic acid in a multicellular tumor spheroid model for squamous carcinoma of the head and neck. Int J Cancer 44:926–932.

Samsel RW, Perelson AS. 1982. Kinetics of rouleau formation. I. A mass action approach with geometric features. Biophys J 37:493–514.

Samsel RW, Perelson AS. 1984. Kinetics of rouleau formation. II. Reversible reactions. Biophys J 45:805–824.

Sauer H, Diedershagen H, Hescheler J, Wartenburg M. 1997. Calcium-dependence of hydrogen peroxide-induced c-fos expression and growth stimulation of multicellular prostate tumor spheroids. FEBS Lett 419:201–205.

Sauer H, Hofmann C, Wartenberg M, Wobus AM, Hescheler J. 1998. Spontaneous calcium oscillations in embryonic stem cell-derived primitive endodermal cells. Exp Cell Res 238:13–22.

Schwachoefer JHM, Crooijmans RPMA, Hoogenhout J, Kal HB, Theeuwes AGM. 1991. Sublethal damage repair in multicellular spheroids from a human melanoma line: Relationship to the size at irradiation. Cancer Ther Contr 1:293–308.

Smoluchowski MV. 1917. Versuch einer mathematischen theorie der koagulationskinetik kolloider loesungen. Z Phys Chem 92:129–168.

Stokes CL, Lauffenburger DA, Williams SK. 1991. Migration of individual microvessel endothelial cells: stochastic model and parameter measurement. J Cell Sci 99:419–430.

Stone KR, Mickey DD, Wunderli H, Mickey GH, Paulson DF. 1978. Isolation of a human prostate carcinoma cell line (DU 145). Int J Cancer 21:274–281.

Sutherland RM. 1988. Cell and environment interactions in tumor microregions: The multicell spheroid model. Science 240:177–184.

Sutherland RM, Durand RE. 1984. Growth and cellular characteristics of multicell spheroids. Cancer Res 95:24–49.

Wigle JC, Freyer JP, Sutherland RM. 1983. Use of a sedimentation column to obtain uniformly sized populations of muticell spheroids. In Vitro 19:361–366.

Yuhas JM, Li AP, Martinez AO, Ladman AJ. 1977. A simplified method for production and growth of multicellular tumor spheroids. Cancer Res 37:3639–3643.

Yuhas JM, Li AP. 1978. Growth fraction as the major determinant of multicellular tumor spheroid growth rates. Cancer Res 38:1528–1532.